ARTICLE IN PRESS

Available online at www.sciencedirect.com

ScienceDirect

Proceedings of the Combustion Institute xxx (2014) xxx–xxx

Proceedings of the Combustion Institute

www.elsevier.com/locate/proci

Numerical experiments on reaction front propagation in *n*-heptane/air mixture with temperature gradient

Peng Dai [a], Zheng Chen [a,b,*], Shiyi Chen [a], Yiguang Ju [c]

[a] *SKLTCS, Department of Mechanics and Engineering Science, College of Engineering, Peking University, Beijing 100871, China*

[b] *Department of Aeronautics and Astronautics, College of Engineering, Peking University, Beijing 100871, China*

[c] *Department of Mechanical and Aerospace Engineering, Princeton University, Princeton, NJ 08544, USA*

Abstract

Usually different autoignition modes can be generated by a hot spot in which ignition occurs earlier than that in the surrounding mixture. However, for large hydrocarbon fuels with negative temperature coefficient (NTC) behavior, ignition happens earlier at lower temperature than that at higher temperature when the temperature is within the NTC regime. Consequently, a cool spot may also result in different autoignition modes. In this study, the modes of reaction front propagation caused by temperature gradient in a one dimensional planar configuration are investigated numerically for *n*-heptane/air mixture at initial temperature within and below the NTC regime. For the first time, different supersonic autoignition modes caused by a cool spot with positive temperature gradient are identified. It is found that the initial temperature gradient has strong impact on autoignition modes. With the increase of the positive temperature gradient of the cool spot, supersonic autoignitive deflagration, detonation, shock-detonation, and shock-deflagration are sequentially observed. It is found that shock compression of the mixture between the deflagration wave and leading shock wave produces an additional ignition kernel, which determines the autoignition modes. Furthermore, the cool spot is compared with the hot spot with temperature below the NTC regime. Similar autoignition modes are observed for the hot and cool spots. Different autoignition modes in the considered simplified configuration are summarized in terms of the normalized temperature gradient and acoustic-to-excitation time scale ratio. It is shown that the transition between different autoignition modes is not greatly affected by the NTC behavior. Therefore, our 1-D simulation indicates that like hot spot, the cool spot may also generate knock in engines when fuels with NTC behavior is used and the temperature is within the NTC regime.

Keywords: Autoignition modes; Cool spot; Temperature gradient; Detonation; *n*-Heptane

1. Introduction

Recently, advanced engine technologies such as homogeneous charge compression ignition (HCCI) and low temperature combustion (LTC)

* Corresponding author at: State Key Laboratory for Turbulence and Complex Systems (SKLTCS), Department of Mechanics and Engineering Science, College of Engineering, Peking University, Beijing 100871, China.

E-mail address: cz@pku.edu.cn (Z. Chen).

http://dx.doi.org/10.1016/j.proci.2014.06.102

1540-7489/

have drawn massive attention due to their excellent performance in efficiency improvement and emission reduction [1]. However, in practical HCCI engines, experiments [2] showed that instead of simultaneous thermal explosion of the entire charge, multiple separated spots first auto-ignite and then are followed by combustion of surrounding charge. These autoignition spots introduce certain modes of reaction front propagation towards unburned gas due to the spatial distribution of charge reactivity.

Zel'dovich [3] first analyzed different modes for propagating combustion waves caused by autoignition in the presence of non-uniform reactivity. Later, other researchers extended Zel'dovich's work using either simplified reaction model [4,5] or detailed chemistry [6–9]. Using 1-D simulation for syngas/air with detailed chemistry and transport, Gu et al. [8] demonstrated that five propagation modes of autoignition front can be initiated by temperature gradient: thermal explosion, supersonic autoignitive deflagration, developing and developed detonation, subsonic autoignitive deflagration, and conventional laminar burning deflagration. They also proposed the limits for detonation initiation in terms of two non-dimensional parameters, namely the normalized temperature gradient (ξ) and the ratio of acoustic time to excitation time (ε) and found a detonation peninsular in the plot of ξ versus ε. The theory of detonation peninsular was further extended in the study of noise and knock (or super-knock) in conventional engines [10–12], turbo-engines [13], and deflagration-to-detonation transition (DDT) experiments [11]. It is noted that in the ξ-ε regime map mentioned above, determination of practical engine conditions usually requires assumptions of temperature gradient and hot spot radius, which make it quantitatively inaccurate. Nevertheless, it provides important qualitative insights on necessary conditions for knock occurrence in practical engines. In addition, Rudloff et al. [12] introduced a new non-dimensional parameter, π, to predict the violence of abnormal combustion in realistic engines along with the location of (ξ, ε) relative to the detonation peninsula.

Previous studies on the autoignition front propagation with reactivity inhomogeneity were mainly focused on simple fuels such as H_2, CO, and CH_4. However, unlike those simple fuels, large hydrocarbons utilized in engines usually have complicated low-temperature chemistry, and therefore manifest complex ignition and burning properties including negative temperature coefficient (NTC) behavior [14–16]. Ignition and reaction wave propagation are influenced by the coupling effects among low- and high-temperature chemistries, transport, and acoustic waves [16]. On the other hand, the non-monotonic dependence of ignition delay time on temperature in NTC regime makes ignition first occur at cooler locations (for example, the position close to the engine wall) instead of hot spots [17]. Zhang et al. [18] studied dimethyl ether auto-ignition in a 1-D laminar situation with temperature inhomogeneities. They observed ignition from cold spots for a mean temperature in NTC regime and assessed the influence of temperature gradient on molecular diffusion effects and pressure fluctuations. Yoo et al. [19] conducted 1-D and 2-D DNS to examine the effects of temperature gradient and turbulence on *n*-heptane/air ignition for various temperatures inside and outside of the NTC regime. However, these two studies only considered subsonic modes of reaction front propagation. In practical Internal Combustion Engines, ignition front propagation might be supersonic when knock or super-knock occurs. Therefore, a comprehensive study on the autoignition front propagation including both subsonic and supersonic modes in temperature inhomogeneity at low temperatures, especially within NTC regime, is needed.

The present work aims to extend the theory on autoignition modes proposed by Zel'dovich [3] and Gu et al. [8] by considering autoignition of *n*-heptane at temperature within the NTC regime in a one dimensional planar configuration. Unlike previous studies considering hot spot, here the autoignition front propagation is initiated by a cool spot in which temperature is lower than surrounding mixture. Different modes of reaction front propagation are observed with the increase of temperature gradient in the cool spot. It is emphasized that unlike hot/cool spot in engines, 1-D planar rather than spherical configuration is considered here and thereby the present results are only of indicative value.

2. Model and specifications

n-Heptane is considered in this study since it is the main component of Primary Reference Fuel (PRF) for gasoline and it has typical two-stage ignition process with low- and high-temperature chemistries as well as NTC behavior [14,15]. In simulation, the skeletal mechanism for *n*-heptane oxidation developed by Liu et al. [14] is used. This mechanism has been demonstrated to be able to accurately predict ignition (including NTC regime) and flame propagation of *n*-heptane/air mixtures at a broad range of temperatures and pressures [14]. Stoichiometric *n*-heptane/air initially at 40 atm is considered in this study. Figure 1(a) shows the homogeneous ignition delay time, τ, as a function of initial temperature, T_0. In the NTC regime, $850 < T_0 < 960$ K, the ignition delay time increases with the initial temperature.

To investigate the different modes of reaction wave propagation, we consider the transient ignition and wave propagation processes in a one-dimensional, planar, adiabatic, closed

Please cite this article in press as: P. Dai et al., *Proc. Combust. Inst.* (2014), http://dx.doi.org/10.1016/j.proci.2014.06.102

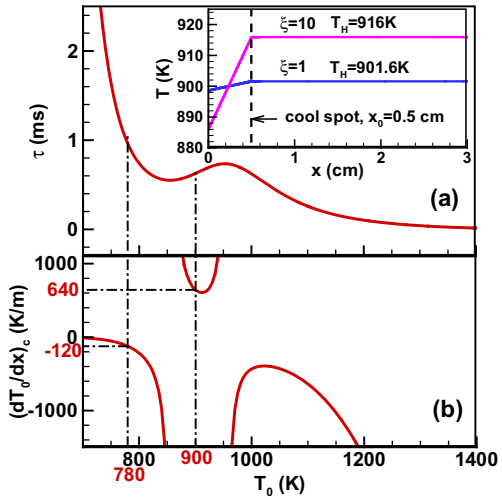

Fig. 1. (a) Ignition delay time and (b) critical temperature gradient as a function of initial temperature for stoichiometric *n*-heptane/air mixture at 40 atm. The inset shows the initial temperature profiles at $T_0 = 900$ K and $\xi = 1$ and 10.

chamber (adiabatic and reflective boundary conditions are adopted for both sides). We limit our focus to laminar combustion regimes and thereby the initial flow is static without turbulence. This simplified configuration is applied to indicate possible behaviors of real systems. As shown in the insert in Fig. 1(a), a cool spot with linear temperature distribution is located on the left side of the domain (i.e. $0 \leqslant x \leqslant x_0$, where x_0 is the size of the cool spot). The temperature outside the cool spot (i.e. $x \geqslant x_0$) is uniform everywhere. The length of the computation domain is 10 cm (i.e. $0 \leqslant x \leqslant 10$ cm) and the size of ignition spot, x_0, varies from 1 mm to 6.1 mm. For the cool spot, the temperature gradient is positive; and it becomes negative once a hot spot is considered.

The critical temperature gradient at which autoignition front propagates at the speed of sound in absence of heat conduction and mass diffusion is [3,8]:

$$\left(\frac{dT_0}{dx}\right)_c = a^{-1}\left(\frac{d\tau}{dT_0}\right)^{-1} \tag{1}$$

where a is local sound speed at which pressure wave propagates. Figure 1(b) shows the critical temperature gradient as a function of initial temperature. Figure 1(b) shows that two singular points exist at the boundaries of NTC regime, and that the critical temperature gradient in NTC regime is positive. Therefore, in NTC regime, locations with lower temperature and proper positive temperature gradient are expected to ignite first and generate developing detonations thereafter. We introduce the non-dimensional temperature gradient, ξ:

$$\xi = \frac{dT_0}{dx} \Big/ \left(\frac{dT_0}{dx}\right)_c \tag{2}$$

where (dT_0/dx) is the temperature gradient within the ignition spot in 1-D simulation. It is noted that the critical temperature gradient is based on the mean temperature of the ignition spot, T_0. As shown in Fig. 1(b), we consider two typical mean temperatures of ignition spot: one is $T_0 = 900$ K within the NTC regime at which a cool spot with positive temperature gradient is established; the other is $T_0 = 780$ K outside the NTC regime at which a hot spot with negative temperature gradient is established. The inset in Fig. 1(a) shows the initial temperature profiles at $T_0 = 900$ K and $\xi = 1$ and 10.

The 1-D autoignition wave propagation is simulated using the in-house code A-SURF (Adaptive Simulation of Unsteady Reactive Flow). A-SURF solves the conservation equations of one-dimensional, compressible, multi-component, reactive flow using the finite volume method. The second-order accurate, Strang splitting fractional-step procedure is utilized to separate the time evolution of the stiff reaction term from that of the convection and diffusion terms. In the first fractional step, the non-reactive flow is solved. The Runge-Kutta, MUSCL-Hancock (with MINBEE flux limiter), and central difference schemes, all of second-order accuracy, are employed for the calculation of the temporal integration, convective flux, and diffusive flux, respectively. The chemistry is solved in the second fractional step using the VODE solver. To maintain adequate numerical resolution of the compression wave, shock wave, and detonation, a multi-level, dynamically adaptive mesh refinement algorithm has been developed and used in A-SURF. The reaction zone, compression wave, shock wave, and detonation wave are always fully covered by the finest meshes of 2 μm and the corresponding time step is 4×10^{-10} s. In the Supplementary document, numerical convergence is demonstrated by further decreasing time step and grid size in simulation. A-SURF has been successfully used in our previous studies on ignition and flame propagation [20–22]. The details on the governing equations, numerical schemes, and code validation can be found in [23–24]. As shown in the Supplementary document, A-SURF can accurately capture shock wave propagation. Moreover, the detonation speed predicted by A-SURF is very close to the Chapman-Jouguet value for detonation speed which shows that A-SURF can capture detonation propagation.

3. Results and discussion

The propagation velocity of autoignition front based on homogeneous ignition condition is [3,8]:

Please cite this article in press as: P. Dai et al., *Proc. Combust. Inst.* (2014), http://dx.doi.org/10.1016/j.proci.2014.06.102

$$u_a^0 = \left(\frac{d\tau}{dx}\right)^{-1} = \left(\frac{d\tau}{dT_0}\frac{dT_0}{dx}\right)^{-1} = a/\xi \quad (3)$$

where the superscript 0 denotes that the velocity is directly deduced from homogeneous results in which heat conduction, mass diffusion, and reacted gas expansion are not taken into consideration. The relation between u_a^0 and sound speed a is only an approximate indicator of the propagation modes of autoignition front since heat conduction and mass diffusion modify the temperature gradient and ignition delay time. For example, one-dimensional simulation [8] shows that developing detonation occurs for a range of ξ lager than unity. In the following we first discuss different autoignition front propagation modes at NTC regime ($T_0 = 900$ K). Stoichiometric *n*-heptane/air mixture initially at 40 atm is considered in this study.

Figure 2 shows the autoignition process at $\xi = 1$ ($dT/dx = 640$ K/m, see Fig. 1b). A supersonic autoignitive deflagration instead of a detonation wave is observed. Because of heat conduction and diffusion of radicals [8], the gradient of the ignition delay, $d\tau/dx$, decreases during induction period, which makes the autoignition front propagates at very high speed of $u_a \sim 4000$ m/s (much greater than the Chapman–Jouguet detonation speed of 1857 m/s). The peak values of temperature and pressure are found to be very close to those of homogeneous ignition at constant volume (3060 K, 146 atm). Therefore, it is a typical supersonic autoignitive deflagration controlled by local autoignition (chemical reactions) instead of transport.

According to Eq. (3), the propagation velocity decreases as the temperature gradient within the cool spot increases. When the normalized temperature gradient reaches a certain value (e.g. $\xi = 3$ for $T_0 = 900$ K), the autoignition wave propagates at a speed close to the sound speed and thereby chemical reaction couples with the pressure wave initiated by local heat release, which results in a developing detonation. Figure 3 shows a typical case of detonation development for $\xi = 10$. It is observed that the detonation wave arises within the cool spot and then propagates into the right until the mixture ahead of it autoignites. After the detonation wave is fully developed (at $t = 665$ μs, denoted by number 2 in Fig. 3), it propagates at a constant speed which is very close to that of C-J detonation speed of 1857 m/s. The maximum pressure (~400 atm) is much higher than that in homogeneous constant-volume ignition (146 atm).

With further increase of temperature gradient, the autoignition front speed decreases according to Eq. (3) such that the pressure wave initiated by the original local thermal explosion decouples with the autoignition front. When $\xi > 19$, the simple C–J detonation shown in Fig. 3 disappears and more complex shock-reaction interaction occurs. A typical case is shown in Fig. 4 for $\xi = 28$. It is observed that the decoupling of pressure wave with the autoignition front occurs at $t = 670$ μs (see the lines denoted by number 1 in Fig. 4).

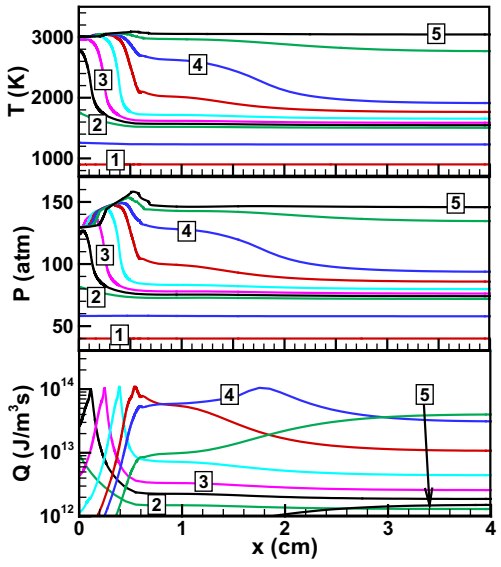

Fig. 2. Temporal evolution of temperature, pressure, and heat release rate distributions for $T_0 = 900$ K, $x_0 = 5$ mm, and $\xi = 1$. The time sequence is 1: 0 μs, 2: 646 μs, 3: 647 μs, 4: 648 μs, 5: 649 μs.

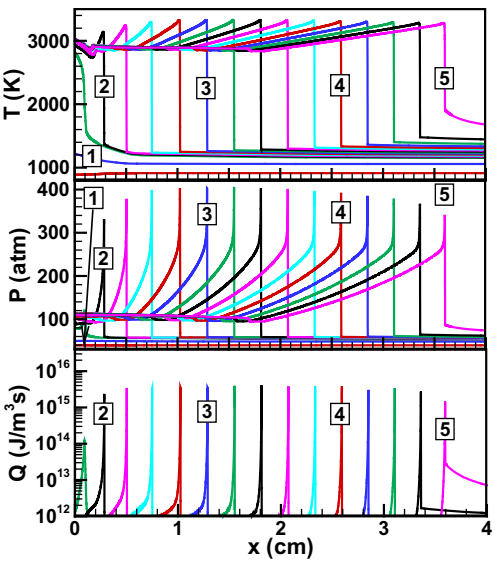

Fig. 3. Temporal evolution of temperature, pressure, and heat release rate distributions for $T_0 = 900$ K, $x_0 = 5$ mm, and $\xi = 10$. The time sequence is 1: 643 μs, 2: 665 μs, 3: 671 μs, 4: 678 μs, 5: 683 μs.

Please cite this article in press as: P. Dai et al., *Proc. Combust. Inst.* (2014), http://dx.doi.org/10.1016/j.proci.2014.06.102

The leading pressure wave propagates towards the right side and eventually evolves into a shock wave (the states before and after the wave are found to satisfy the jump relations for normal shock). Figure 4 indicates that chemical reactions mainly take place at the deflagration wave behind the shock wave and there is no heat release around the shock. However, due to the shock compression, the mixture between the deflagration wave and leading shock wave starts to auto-ignite at $t = 705$ μs (line #2 in Fig. 4) [25]. This eventually evolves into a detonation wave (line #4 in Fig. 4). This phenomenon is similar to the 'explosion in the explosion' observed by Urtiew et al. [26] in their study of DDT except that turbulence is present in their experiments.

Figure 5 shows the evolution of the location and propagation velocity of the reaction front and shock wave for the same case as in Fig. 4. The reaction front consequently manifests as (I) deflagration, (II) autoignition in front of the deflagration, and (III) detonation. The jump of the velocity of reaction front in Fig. 5 is due to fast autoignition of the shock-compressed mixture. At $t = 720$ μs, the reaction front couples with the shock wave and becomes a detonation which propagates to the right at a velocity close to C–J detonation value of 1857 m/s until all the rest of gas auto-ignites at $t = 740$ μs .

Since the mean temperature in the cool spot, T_0, is fixed at 900 K, the lowest temperature at $x = 0$, T_L, and highest temperature at $x = x_0$, T_H, (see the insert in Fig. 1a) decreases and increases, respectively, with the temperature

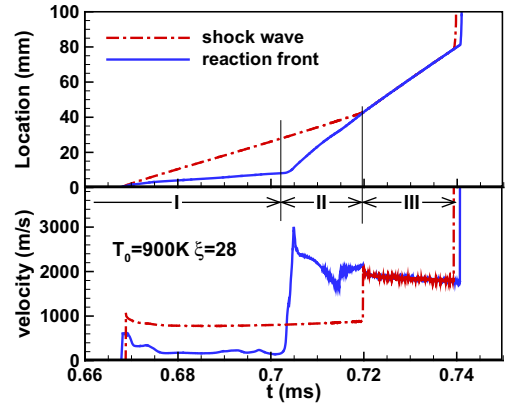

Fig. 5. Temporal evolution of location and velocity of the reaction front and shock wave for the same case as in Fig. 4.

gradient. When the temperature gradient is large (i.e. $\xi > 32$), the lowest temperature at $x = 0$ is below 850 K which is lower boundary of NTC regime. Consequently, auto-ignition does not happen sequentially from the left side to the right side within the cool spot. Figure 6 shows the results for $\xi = 45$. It is observed that autoignition first occurs in the middle of the cool spot (see line #1) instead of at $x = 0$. This ignition kernel forms two deflagration and pressure waves propagating towards the left and right sides. The left-propagating pressure wave quickly reaches the wall and gets reflected. Therefore, at $t = 675$ μs (line #2 in Fig. 6), a two-step like temperature profile is

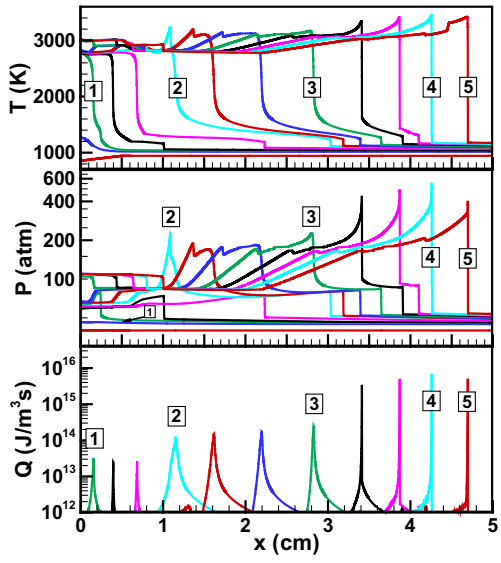

Fig. 4. Temporal evolution of temperature, pressure, and heat release rate distributions for $T_0 = 900$ K, $x_0 = 5$ mm, and $\xi = 28$. The time sequence is 1: 670 μs; 2: 705 μs; 3: 712 μs; 4: 720 μs; 5: 722 μs.

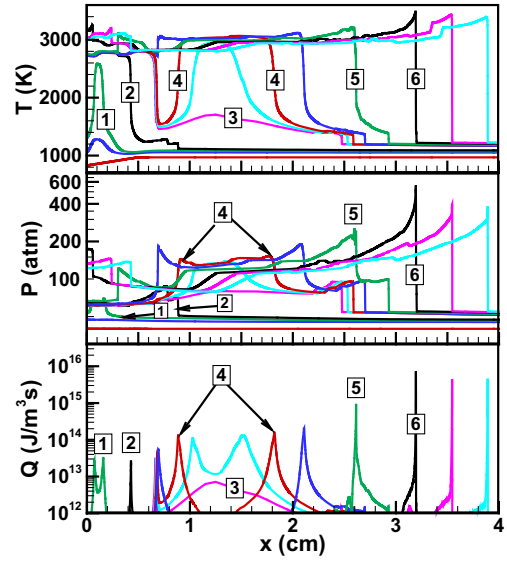

Fig. 6. Temporal evolution of temperature, pressure, and heat release rate distributions for $T_0 = 900$ K, $x_0 = 5$ mm, and $\xi = 45$. The time sequence is 1: 666 μs; 2: 675 μs; 3: 694 μs; 4: 695 μs; 5: 699 μs; 6: 701 μs.

Please cite this article in press as: P. Dai et al., *Proc. Combust. Inst.* (2014), http://dx.doi.org/10.1016/j.proci.2014.06.102

observed ahead of the deflagration wave. This particular pressure wave assemble finally evolves in to a single shock wave. Like the case in Fig. 4, autoignition occurs in the shock-compressed mixture between the deflagration wave and shock wave at $t = 694$ μs (line #3 in Fig. 6). The non-monotonic temperature distribution for the shock-compressed mixture is the consequence of two competing factors: although the left part of the mixture is compressed by the shock earlier, the strength of the shock is weaker compared with the later one which compresses the right part of the mixture since the shock wave intensifies itself during propagation. Consequently, some point in the middle ignites first compared with the surrounding substance. This autoignition kernel again forms two deflagration and pressure waves propagating towards the left and right sides (line #4 in Fig. 6). The deflagration wave moving toward the left consumes all reactants therein. On the other hand, the deflagration wave propagating toward the right evolves into a detonation wave, similar to the case shown in Fig. 4.

With further increase in temperature gradient, the temperature outside the cool spot finally exceeds the upper boundary of NTC regime and eventually the mixture outside the cool spot auto-ignites first. Therefore, for very large ξ, the cool spot and the surrounding mixture ignite almost simultaneously (the temporal evolution of temperature, pressure, and heat release rate distributions is not plotted due to space limit). This occurs around $\xi > 55$ for $T_0 = 900$ K and $x_0 = 5$ mm. With the decrease of the cool spot size, x_0, the critical normalized temperature gradient, ξ, increases (e.g. $\xi > 110$ for $x_0 = 2$ mm).

In summary, three autoignition modes are observed for a cool spot with temperature in NTC regime: I, supersonic autoignitive deflagration (Fig. 2); II, detonation (Fig. 3); and III, shock- detonation (Figs. 4 and 6). Figure 7 shows the temperature gradient ranges for different autoignition modes at $T_0 = 900$ K and $x_0 = 2$ mm and 5 mm. It is noted that autoignition mode III includes two cases which differ from each other in terms of the monotonicity of temperature profile in cool spot after its autoignition (III-1, monotonic, see Fig. 4; and III-2, non-monotonic, see Fig. 6). For $x_0 = 5$ mm, the autoignition advance of cool spot compared with the surrounding mixture vanishes when $\xi > 55$ while the ignition advantage of cool spot with $x_0 = 2$ mm always exists in the temperature gradient range shown in Fig. 7.

In order to further reveal the influence of initial temperature gradient within cool spot on the autoignition front propagation, Fig. 8 shows temporal evolution of reaction front location and velocity for different values of normalized temperature gradient, ξ, with $x_0 = 5$ mm. The dashed horizontal lines represent C–J detonation velocity

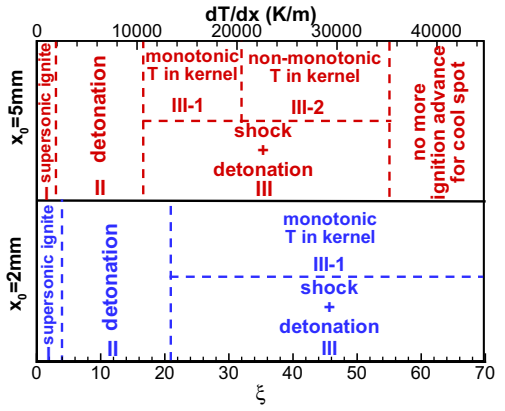

Fig. 7. Autoignition modes at different temperature gradients and cool spot sizes with $T_0 = 900$ K.

of 1857 m/s. When ξ is very small, the autoignition wave propagates supersonically ($u_a \sim 4000$ m/s for $\xi = 1$) and thermal explosion occurs soon after the ignition of cool spot. With the increase of ξ ($\xi = 5$–19), a detonation develops and maintains itself even outside of the cool spot until thermal explosion occurs. A further increase of ξ, however, leads to decouple between the leading shock wave and the reaction zone. Autoignition kernel appears in the mixture between the deflagration wave and leading shock (Figs. 4 and 6). The appearance of this kernel is manifested in Fig. 8 by the sudden jump of reaction front velocity for $\xi = 23$ and the jump of both reaction front location and velocity for $\xi = 38$. The deflagration wave formed by the additional ignition kernel soon evolves into a detonation and propagates rightward until thermal explosion of the system occurs.

Although cases with $x_0 = 5$ mm shown in Fig. 8 clearly show the propagating process of both detonation and shock-detonation, the fourth mode of shock-deflagration does not exist in this config-

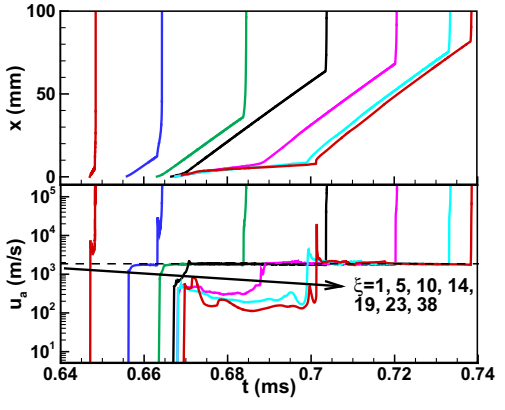

Fig. 8. Temporal evolution of location and velocity of the reaction fronts for different ξ ($T_0 = 900$ K, $x_0 = 5$ mm).

Please cite this article in press as: P. Dai et al., *Proc. Combust. Inst.* (2014), http://dx.doi.org/10.1016/j.proci.2014.06.102

uration due to the limitation of upper boundary of the NTC regime. For cases with smaller cool spot ($x_0 = 2$ mm) and thus smaller temperature difference, all the four autoignition modes including supersonic autoignitive deflagration, detonation, shock-detonation and shock-deflagration are observed. It is noted that the last mode is quite similar to the shock-detonation, except that its velocity never reaches C–J value (i.e. supersonic deflagration) before thermal explosion. In addition, its maximum pressure (~200 atm) is much lower than that of detonation case.

Unlike the cases studied by Gu et al. [8] and Bradley et al. [10], the decouple of pressure wave and reaction zone does not necessarily lead to the failure of detonation development here. This is because the spherical geometry was considered therein while the planar configuration is considered in the present study. In Fig. 8, the subsonic deflagration waves at large ξ before additional ignition kernels appear (velocity and location jump) are basically the same as the 'subsonic deflagration' in Ref. [8]. The autoignition caused by wave-compression was also observed by Weber et al. [7] in H_2/O_2 mixture. They emphasized that this situation happens only when the mixture temperature outside the hot spot is high enough. Considering that the mixture is above 1000 K before the shock wave arrives (see Figs. 4 and 6), shock-compression in this work plays a dominant role in changing autoignition modes. Similar conclusion was also drawn in a recent review paper [25] on the interactions between flame propagation and pressure waves. In addition, autoignition front of deflagration wave caused by shock wave was observed by Urtiew et al. [26] in their early experimental study on DDT. However, the so-called 'explosion in the explosion' in their experiment was the result of turbulence, wall effects, gas dynamics (transverse shock wave) and combustion chemistry, which was intrinsically multi-dimensional. Bradley [11] analyzed this experimental phenomenon in his 'detonation peninsular' framework using one-dimensional theory considering turbulent flame and the good agreement was achieved. Therefore, the shock-detonation and shock-deflagration modes observed in this work could be instructive for relevant experimental and multi-dimensional simulation observations despite of its one-dimensional and laminar nature.

Besides the cool spot within NTC regime, we also investigate flame propagation caused by hot spot outside NTC regime. A low temperature, $T_0 = 780$ K, is chosen as the mean temperature within the hot spot, which corresponds to a critical temperature gradient of -120 K (see Fig. 1). The negative value indicates that a hot spot with high temperature rather than a cool spot can generate propagating autoignition wave. It is found that despite of the different dependence of ignition

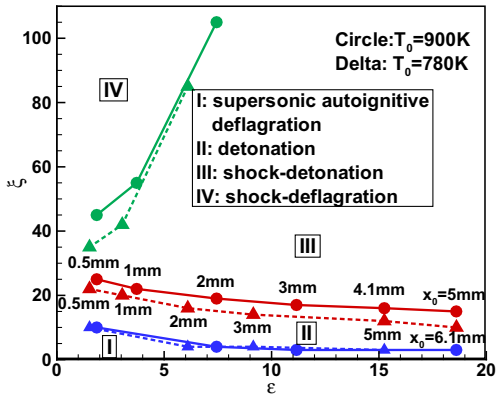

Fig. 9. Autoignition modes initiated by a cool spot ($T_0 = 900$ K) and a hot spot ($T_0 = 780$ K) in terms of ξ and ε.

delay time on temperature within and outside the NTC regime, the hot and cool spots show similar autoignition modes with the increase of the normalized temperature gradient, ξ. Figure 9 summarizes the autoignition modes in terms of ξ and ε. Following Gu et al. [8], ε is the ratio of acoustic time (x_0/a) to excitation time τ_e (defined as the time interval between 5% and maximum heat release rate), which assesses the rapidity of reaction energy release. It is observed that the boundaries between two adjacent modes for the cool spot ($T_0 = 900$ K) are close to those for the hot spot ($T_0 = 780$ K). This implies that the NTC behavior does not significantly change the autoignition modes as long as ξ and ε are fixed. Moreover, Fig. 9 shows that ξ separating autoignition modes II and III slightly decreases with ε, implying that a larger ε (or a larger x_0 for fix cool/hot spot mean temperature T_0) promotes the decouple of pressure wave from reaction zone. With the increase of ε, the range for ξ in autoignition mode III expands greatly, indicating that the compression effect of shock wave is enhanced. This is due to more rapid reaction energy release at higher ε which enhances the strength of pressure wave.

4. Conclusions

Different autoignition modes caused by temperature gradient are investigated numerically in a one dimensional planar configuration for *n*-heptane/air mixture at initial temperature within and below the NTC regime. In previous studies, hot spot with negative temperature gradient was used to generate different autoignition modes. Here autoignition modes caused by a cool spot with positive temperature gradient (the initial temperature is within NTC regime) are studied and different supersonic autoignition modes are identified. The initial temperature gra-

Please cite this article in press as: P. Dai et al., *Proc. Combust. Inst.* (2014), http://dx.doi.org/10.1016/j.proci.2014.06.102

dient is shown to have a great impact on autoignition modes. With the increase of the temperature gradient of the cool spot, four autoignition modes are identified: supersonic autoignition deflagration, detonation, shock-detonation, and shock-deflagration. It is found that in the present configuration, the shock compression of the mixture between the deflagration wave and leading shock wave produces an additional ignition kernel, which evolves into either a detonation wave or a supersonic deflagration wave. Therefore, shock-compression could be an important factor determining the autoignition modes. Furthermore, the hot spot with temperature below the NTC regime is also studied and similar autoignition modes are observed for the hot and cool spots. Different autoignition modes in one dimensional planar configuration are summarized in terms of two normalized variables ξ (normalized temperature gradient) and ε (the ratio between acoustic time and excitation time). It is shown that the NTC behavior does not greatly change the autoignition modes as long as ξ and ε are fixed. Therefore, simulations in the present academic configuration suggest that like hot spot, the cool spot may also generate knock in engines when fuels with NTC behavior is used and the temperature is within the NTC regime.

Acknowledgement

ZC would like to thank the support from National Natural Science Foundation of China (Nos. 51322602 and 51136005) and State Key Laboratory of Engines at Tianjin University (No. K2014-01). YJ would like to thank the Army Research Grant W911NF-12-1-0167 for multi-scale modeling. Helpful discussions with Professor Yipeng Shi and Mr. Bin Bai at Peking University were appreciated.

Appendix A. Supplementary data

Supplementary data associated with this article can be found, in the online version, at http://dx.doi.org/10.1016/j.proci.2014.06.102.

References

[1] J.E. Dec, *Proc. Combust. Inst.* 32 (2009) 2727–2742.
[2] J. Nygren, J. Hult, M. Richter, M. Aldén, M. Christensen, A. Hultqvist, B. Johansson, *Proc. Combust. Inst.* 29 (2002) 679–685.
[3] Y.B. Zel'dovich, *Combust. Flame* 39 (1980) 211–214.
[4] A.M. Khokhlov, E.S. Oran, J.C. Wheeler, *Combust. Flame* 108 (1997) 503–517.
[5] D. Bradley, *J. Chem. Soc. Faraday Trans.* 92 (1996) 2959–2964.
[6] A.E. Lutz, R.J. Kee, J.A. Miller, H.A. Dwyer, A.K. Oppenheim, *Proc. Combust. Inst.* 22 (1989) 1683–1693.
[7] H.J. Weber, A. Mack, P. Roth, *Combust. Flame* 97 (1994) 281–295.
[8] X.J. Gu, D.R. Emerson, D. Bradley, *Combust. Flame* 133 (2003) 63–74.
[9] M.A. Liberman, A.D. Kiverin, M.F. Ivanov, *Phys. Rev. E* 85 (2012).
[10] D. Bradley, G.T. Kalghatgi, *Combust. Flame* 156 (2009) 2307–2318.
[11] D. Bradley, *Philos. Trans. R. Soc. A* 370 (2012) 689–714.
[12] J. Rudloff, J.M. Zaccardi, S. Richard, J.M. Anderlohr, *Proc. Combust. Inst.* 34 (2013) 2959–2967.
[13] G.T. Kalghatgi, D. Bradley, *Int. J. Engine Res.* 13 (2012) 399–414.
[14] S.L. Liu, J.C. Hewson, J.H. Chen, H. Pitsch, *Combust. Flame* 137 (2004) 320–339.
[15] C.K. Law, P. Zhao, *Combust. Flame* 159 (2012) 1044–1054.
[16] Y.G. Ju, W.T. Sun, M.P. Burke, X.L. Gou, Z. Chen, *Proc. Combust. Inst.* 33 (2011) 1245–1251.
[17] M. Schreiber, A. Sadat Saka, C. Poppe, J.F. Griffiths, P. Halford-Maw, D.J. Rose, SAE-932758, (1993).
[18] H.Y. Zhang, E.R. Hawkes, J.H. Chen, S. Kook, *Proc. Combust. Inst.* 34 (2013) 803–812.
[19] C.S. Yoo, T.F. Lu, J.H. Chen, C.K. Law, *Combust. Flame* 158 (2011) 1727–1741.
[20] Z. Chen, M.P. Burke, Y.G. Ju, *Proc. Combust. Inst.* 33 (2011) 1219–1226.
[21] Z. Chen, *Combust. Flame* 158 (2011) 291–300.
[22] W.K. Zhang, Z. Chen, W.J. Kong, *Combust. Flame* 159 (2012) 151–160.
[23] Z. Chen, M.P. Burke, Y.G. Ju, *Proc. Combust. Inst.* 32 (2009) 1253–1260.
[24] Z. Chen, *Combust. Flame* 157 (2010) 2267–2276.
[25] J. Pan, G. Shu, H. Wei, *Combust. Sci. Technol.* 186 (2014) 192–209.
[26] P.A. Urtiew, A.K. Oppenheim, *Proc. R. Soc. London, A* 295 (1966) 13–28.